

RB5 Low-Cost Explorer: Implementing Autonomous Long-Term Exploration on Low-Cost Robotic Hardware

Adam Seewald¹, Marvin Chancán¹, Connor M. McCann², Seonghoon Noh¹, Omeed Fallahi¹, Hector Castillo¹, Ian Abraham¹, and Aaron M. Dollar¹

Abstract—This systems paper presents the implementation and design of RB5, a wheeled robot for autonomous long-term exploration with fewer and cheaper sensors. Requiring just an RGB-D camera and low-power computing hardware, the system consists of an experimental platform with rocker-bogie suspension. It operates in unknown and GPS-denied environments and on indoor and outdoor terrains. The exploration consists of a methodology that extends frontier- and sampling-based exploration with a path-following vector field and a state-of-the-art SLAM algorithm. The methodology allows the robot to explore its surroundings at lower update frequencies, enabling the use of lower-performing and lower-cost hardware while still retaining good autonomous performance. The approach further consists of a methodology to interact with a remotely located human operator based on an inexpensive long-range and low-power communication technology from the internet-of-things domain (i.e., LoRa) and a customized communication protocol. The results and the feasibility analysis show the possible applications and limitations of the approach.

Code—The open-source software stack is made available on the project repository webpage[†].

I. INTRODUCTION

The promise of autonomous long-term robotic exploration is currently being restricted in part by the expense of the required sensing, computing, and mechanical hardware. This cost is related to the computational intensity of most common navigation and communication approaches [1, 2], which significantly increases for outdoor terrains. Addressing this challenge, we introduce techniques to reduce update frequencies and enhance the communication capabilities of existing approaches. By loosening the required update frequencies and communication requirements, our methods enable the use of lower-performing and lower-cost hardware while still retaining good autonomous performance.

Recent efforts in this direction include low-cost robots that, e.g., exploit sensing capabilities of commercial smartphones [3, 4] but lack crucial components for autonomous long-term exploration such as terrain adaptability [3, 5], outdoor navigation [4, 6], etc. Furthermore, in areas that are challenging to traverse, state-of-the-art approaches rely on

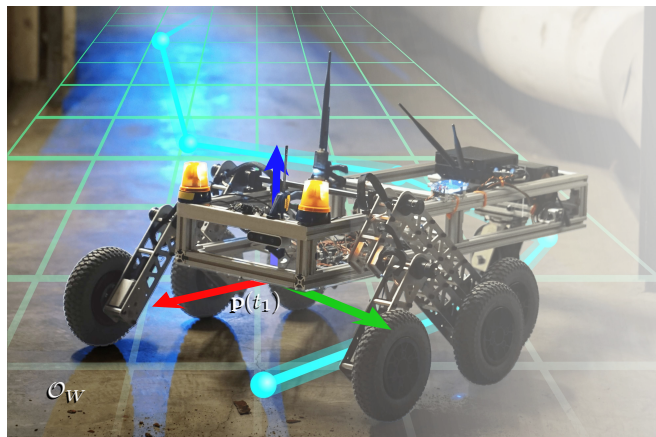


Fig. 1: RB5 low-cost wheeled robotic explorer. A robot needs to explore its surroundings with fewer and cheaper sensors – the picture illustrates RB5, our experimental wheeled robotic platform that carries an RGB-D camera and low-power computing hardware to derive an exploratory coverage path.

humans for supervision and high-level decision-making [7–9]. As a result, robots often operate close to humans or require expensive network equipment such as a mesh of communication devices [10, 11] and existing network infrastructure [12, 13], thereby restricting autonomous exploration to indoor settings only [14–17]. Our methodology exploits LoRa – an inexpensive long-range and low-power communication technology [18] from the internet-of-things domain – and a customized communication protocol. This allows a human to intervene when the robot is unable to move with the local sensory information.

For visual sensing, our approach maintains a low sensory footprint with low-cost components: an RGB depth (RGB-D) camera to sense the environment. Most approaches tackling autonomous exploration use costly equipment such as 3D LiDARs [7–11, 19–21] and laser range finders [22, 23] instead. Even though approaches that utilize cheaper sensors, such as RGB-D cameras [24–26], RGB cameras [20], sonars [3, 4], and 2D LiDARs are studied [5], they often operate along more expensive hardware [20] or indoors only [24] and have limited autonomy [25] or obstacle avoidance features [3, 4].

From a software perspective, recent efforts tackle autonomous exploration with prior learning [27] or run on multiple robots [7, 8, 10], whereas approaches that require fewer computing resources are scarce [3, 6, 21, 24]. Although some less computationally demanding approaches, such as those based on frontiers [8, 21, 22], graphs [7, 10, 20], grids [9, 17], and random trees are studied, mixed approaches (i.e., a combination of the previous approaches) are pre-

This work was partly supported by Yale University and a gift from the Boston Dynamics AI Institute.

¹A. S., M. C., S. N., O. F., H. C, I. A., and A. M. D. are with the Department of Mechanical Engineering and Materials Science, Yale University, CT, USA. Email: adam.seewald@yale.edu;

²C. M. M. is with the School of Engineering and Applied Sciences, Harvard University, MA, USA, but the work was performed while affiliated with Yale University.

[†]github.com/adamseew/rb5

ferred [23–25, 27, 28]. In the presence of diverse sensing modalities, e.g., involving raw sensory data, topologies, semantics, etc., and outdoor environments [2, 21], mixed approaches maximize performance and resources [2, 24]. Our methodology is a mixed approach: a frontier- and sampling-based method that extends exploration with a path-following vector field from the aerial robotics domain [29–31]. It exploits the scarcity of resources while still running with good autonomy and obstacle avoidance features. Furthermore, our approach derives the robot’s position using a state-of-the-art simultaneous localization and mapping (SLAM) algorithm [32] and can operate in both unknown and GPS-denied environments. This allows the robot to explore its surroundings for longer and at lower update frequencies, utilizing cheaper computing hardware.

Utilizing these components with the open-source robot operating system (ROS) middleware, we additionally build a low-cost robotic platform – RB5 in Figure 1, a wheeled mobile robot with rocker-bogie suspension – capable of exploring indoor and outdoor environments autonomously. Comparable platforms in the literature comprise two degrees of freedom suspension with pivots [6, 33] and provide rough terrain static adaptability. They are cheaper than, e.g., legged robots in terms of the price of sensors and operation, as they avoid obstacles without costly computations for gait adaptation and planning [3]. The approach is generic in terms of portability to other mobile robots with price and computational constraints, but we target use cases where cheaper robotic explorers are preferred. These include nature conservation and surveying efforts [34] and education [26, 35]. The open-source software stack to replicate our approach is made available on the project repository webpage[†].

The main **contributions** of this systems paper are (i) the *implementation and design of a low-cost robot for autonomous long-term exploration* and (ii) its *feasibility and limitations analysis*. We demonstrate the exploration performance and obstacle avoidance features with a set of indoor and outdoor experiments in Section IV and discuss the limitations of our low-cost exploration in Sec. V. The remainder of the paper is then structured as follows: Sec. II formalizes the problem of autonomous exploration, Sec. III describes the approach from the software and hardware standpoints, and Sec. VI concludes and provides future perspectives.

II. PROBLEM DESCRIPTION

The problem considered in this work is that of exploring an unknown bounded space, i.e., visiting every point within. The robot is free to move except for some possible obstacles. Formally, the problem is that of exploring a bounded volume $\mathcal{Q} \subseteq \mathbb{R}^3$ with respect to an inertial navigation frame \mathcal{O}_W . If the notation $[n]$ denotes a set of positive naturals up to $n \in \mathbb{N}_{>0}$ and $[n]_{>0}$ of strictly positive naturals, we are interested in collision-free trajectories that explore \mathcal{Q} and avoid n obstacles $\mathcal{Q}^{O_i} \subset \mathbb{R}^3, i \in [n]_{>0}$. We can approximate the space that delimits \mathcal{Q} and \mathcal{Q}^{O_i} for each i with a set of vertices within which the two sets are contained.

Problem (Exploration). Consider sets of vertices $V := \{\mathbf{v}_1, \mathbf{v}_2, \dots\}$, $O_i := \{\mathbf{o}_{i,1}, \mathbf{o}_{i,2}, \dots\}$ with $\mathbf{v}_j, \mathbf{o}_{i,k} \in \mathbb{R}^2, \forall j \in [|V|], k \in [|O_i|]$ points w.r.t. \mathcal{O}_W . Let V enclose \mathcal{Q} , $O_i \mathcal{Q}^{O_i}$ per each $i \in [n]_{>0}$. The *exploration problem* is the problem of finding the coverage that visits every point $\mathbf{p} \in \mathcal{Q} \cap \mathcal{Q}^{O_1} \cap \mathcal{Q}^{O_2} \cap \dots \cap \mathcal{Q}^{O_n} =: \mathcal{Q}^V$.

Here the notation $|\cdot|$ denotes the cardinality and \mathbb{R}, \mathbb{Z} are reals and integers. Bold notation is used for vectors.

Let ϕ be a path function, i.e., a function the robot tracks as it explores its surroundings in \mathcal{Q}^V , avoiding obstacles \mathcal{Q}^{O_i} .

Definition II.1 (Path function). $\phi : \mathbb{R}^2 \rightarrow \mathbb{R}$ is a two-dimensional continuous and differentiable *path function* of the x, y components of \mathbf{p} .

Definition II.2 (Coverage). Given a tuple with a path function and its time component, $\langle \phi, t \rangle$, the *coverage* is the collection of multiple tuples.

The exploration approach (see Sec. III-A) derives ϕ at each time step and adds it to the global “coverage stack.” The process ends once \mathcal{Q}^V is covered.

III. SYSTEMS APPROACH

In this section, we detail the implementation and design choices in terms of our software and low-cost hardware for autonomous long-term exploration in Sec. III-A and III-B respectively.

A. Autonomous exploration

Our software stack consists of a mixed approach that combines frontier- and sampling-based methods. Here, with frontiers, we indicate boundaries between known and unknown space [2, 20].

Our approach evaluates local frontiers at each step, samples the environment, and determines feasible candidate path functions ϕ that intersect \mathcal{Q}^V (see Definition II.1). The next ϕ is selected so that the frontier is largest, but other cost functions are possible (see Sec. VI). The collection of the candidate path functions forms the coverage (see Def. II.2). The approach then derives a path-following vector field that points to ϕ at any point and guides the robot utilizing the gradient descent algorithm. This allows the robot to, e.g., follow the coverage path for longer and in real-time compared to approaches that utilize frontiers only, decreasing computational requirements (see Sec. IV).

To derive the path-following vector field, let the gradient of ϕ be defined

$$\nabla \phi := \begin{bmatrix} \partial \phi / \partial \mathbf{p}_x \\ \partial \phi / \partial \mathbf{p}_y \end{bmatrix}, \quad (1)$$

where $\partial \phi / \partial \mathbf{p}$ is the partial differential, and $\mathbf{p}_x, \mathbf{p}_y$ are the x and y components of \mathbf{p} . The path-following vector field points in the direction where ϕ maximally locally increases. To assign the direction to each point, we use the construct of vector fields, which is common in other motion planning literature [30, 36]

$$\Phi(t, \phi) := \bigcup_{\mathbf{p}(t) \in \mathcal{Q}} \nabla \phi(\mathbf{p}(t)). \quad (2)$$

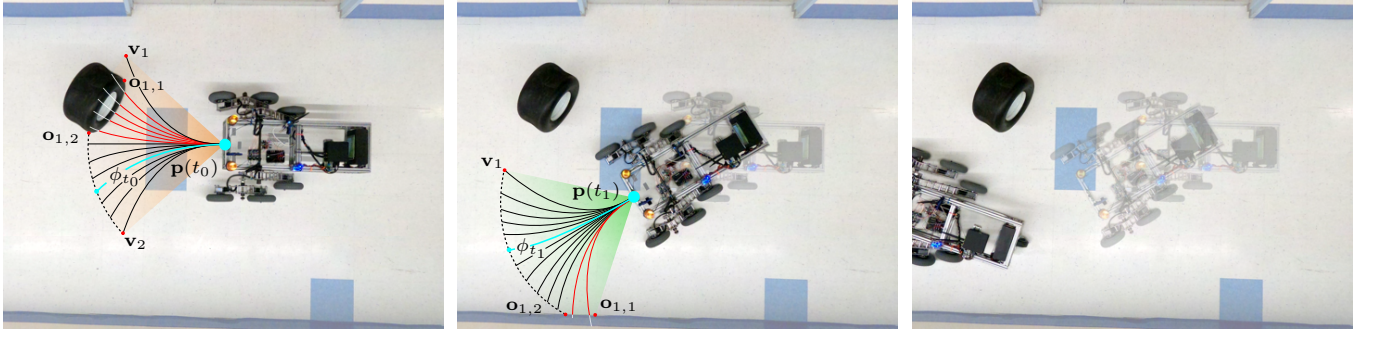


Fig. 2: **Detail of our autonomous exploration methodology.** The approach consists of the robot sampling the environment and searching for obstacles and unexplored areas. The approach clusters the two groups into vertex sets and builds candidate path functions. From these, it selects the trajectory w.r.t. a given cost function and iterates the operation at each step. In between the iterations, it tracks the trajectory, saving computational and sensing resources.

Fig. 2: **Detail of our autonomous exploration methodology.** The approach consists of the robot sampling the environment and searching for obstacles and unexplored areas. The approach clusters the two groups into vertex sets and builds candidate path functions. From these, it selects the trajectory w.r.t. a given cost function and iterates the operation at each step. In between the iterations, it tracks the trajectory, saving computational and sensing resources.

Algorithm 1 Derivation of the exploration coverage $\langle \phi, t \rangle$

```

1: for all  $t \in \mathcal{T}$  do
2:   if  $\mathcal{P} \cap \mathcal{Q} = \emptyset$  then return  $\langle \phi, t \rangle$ 
3:    $\mathcal{Q}_t^V := \{O_{1,t}, O_{2,t}, \dots, O_{n,t}, V_t\} \leftarrow$  sensor readings
4:   if  $\mathcal{Q}_t^V \neq \mathcal{Q}_{t-1}^V$  then
5:      $\{\phi_{1,t}, \phi_{2,t}, \dots\} \leftarrow \phi$ s in Def. II.1, inters.  $\mathcal{Q}^V \cap \Psi(\mathcal{Q}_t^V)$ 
6:     if  $\phi_t := \{\phi_{1,t}, \phi_{2,t}, \dots\} = \emptyset$  then the robot is stuck
7:     else
8:        $\phi_t \leftarrow \arg \max_{\phi} l(\phi_t, t, \mathcal{Q}_t^V)$  in Eq. (7)
9:        $\langle \phi, t \rangle \leftarrow \langle \phi, t \rangle \cup \langle \phi_t, t \rangle$  in Def. II.2
10:       $\mathcal{P} \leftarrow \mathcal{P} \cup \Psi(\mathcal{Q}_t^V)$ 
11:    end if
12:  end if
13:   $\varphi(t, \mathbf{p}(t)) \leftarrow \varphi(t-1, \mathbf{p}(t-1)) + \theta \Delta \phi(\mathbf{p}(t))$  in Eq. (3)
14: end for

```

We modify the vector field in Equation (2) to point to the contour of the path function ϕ rather than its local maxima, as proposed in [30]

$$\Delta \phi(\mathbf{p}(t)) := E \nabla \phi(\mathbf{p}(t)) - k_e \phi(\mathbf{p}(t)) \nabla \phi(\mathbf{p}(t)), \quad (3)$$

where $E \nabla \phi$ points perpendicularly to the gradient and $\phi \nabla \phi$ to ϕ at $k_e \in \mathbb{R}_{>0}$ rate. E is the following direction, i.e.,

$$E = \begin{bmatrix} 1 & 0 \\ 0 & -1 \end{bmatrix}, \quad (4)$$

is counterclockwise and $-E$ clockwise directions.

Let the path-following equivalent of Eq. (2) be

$$\Phi_{\phi}(t, \phi) := \bigcup_{\mathbf{p}(t) \in \mathcal{Q}} \Delta \phi(\mathbf{p}(t)). \quad (5)$$

The path-following vector field is summarized in the pseudo-code in Algorithm 1, with the gradient descent in Line 13. The vector $\varphi \in \mathbb{R}^2$ points the robot in the direction of the path function ϕ with a scalar step size $\theta \in \mathbb{R}_{>0}$. The algorithm runs at each time step in \mathcal{T} , but practically there might be different time steps at different times (see Sec. IV). In Line 2, the algorithm evaluates if the bounded volume \mathcal{Q} is covered utilizing $\mathcal{P} \subseteq \mathbb{R}^3$ updated in Line 10, where the function $\Psi: \mathbb{R}^{2n} \times \mathbb{R}^2 \rightarrow \mathbb{R}^{3n} \times \mathbb{R}^3$ maps the vertices to the volume. The vertices of the local free space \mathcal{Q}_t^V in Line 3

are derived from sensor readings, assuming the presence of an RGB-D camera. The approach reads the camera's point cloud, clustering the obstacles $O_{1,t}, O_{2,t}, \dots$ by checking if the distance between consecutive points in space is within a given threshold $\varepsilon \in \mathbb{R}_{>0}$. The vertices of the free space at time instant t , V_t are simply the limits of the sensor's field of view.

The remaining lines compute the feasible path functions $\{\phi_{1,t}, \phi_{2,t}, \dots\}$ by intersecting the local free space $\Psi(\mathcal{Q}_t^V)$ with possible candidate trajectories that have their final points laying at the edges of \mathcal{Q}_t^V , i.e., splines of the form

$$a(x - \mathbf{p}_x)^3 + b(x - \mathbf{p}_x)^2 + c(x - \mathbf{p}_x) + d - y = 0, \quad (6)$$

where $a, b, c \in \mathbb{R}$ are the coefficients of the spline. The best trajectory is then derived via the cost function l in Line 8, utilizing the intersection of the largest frontier. Formally

$$l := \left\{ \|\mathbf{p}_1 - \mathbf{p}_2\| \mid \exists \mathbf{p}_1, \mathbf{p}_2 \in \Psi(\mathcal{Q}_t^V), i \in \llbracket \phi_t \rrbracket \right. \\ \left. \text{s.t. } \mathbf{p}_1 \neq \mathbf{p}_2, \phi_{i,t}(\mathbf{p}_1 - \mathbf{p}_2) \leq 0 \right\}, \quad (7)$$

where the operator \leq evaluates ϕ on a given $\varepsilon \in \mathbb{R}_{>0}$, i.e., $|\phi_{i,t}(\mathbf{p}_1 - \mathbf{p}_2)| \leq \varepsilon$ and in such a way that the middle path functions of the largest subset of the contiguous path functions are selected preferably, e.g., if the largest subset is $\{\phi_{1,t}, \phi_{2,t}, \dots, \phi_{5,t}\}$, $\phi_{3,t}$ is selected. In this way, if there are no obstacles, Eqs. (6-7) are such that ϕ is a line parallel to the direction of travel.

The algorithm is illustrated in Fig. 2. At each iteration, the robot samples the environment and derives a set of candidate path functions $\{\phi_{1,t}, \phi_{2,t}, \dots\}$. If there is no obstacle ahead, the optimal function per iteration ϕ_t is a line parallel to the robot's direction of travel (see Fig. 2c). If there are obstacles, the approach selects the trajectory via the cost function l , ϕ_t , which goes through the middle of the largest frontier (see Fig. 2a and 2b for obstacles "wheel" and "wall").

The algorithm provides a way to explore space \mathcal{Q} and avoid obstacles \mathcal{Q}^{O_i} . Nevertheless, there are configurations at which there are no feasible trajectories, i.e., if $\{\phi_{1,t}, \phi_{2,t}, \dots\} = \emptyset$ in Line 6. In this scenario, our approach allows a human to intervene via wireless or LoRa communication technology. The robot can be then teleoperated

over long distances – studies from the internet-of-things domain [18] report a range of up to five kilometers in an urban setting – and with inexpensive hardware equipment (two LoRa bundles). The approach we propose utilizes a web interface to parse human commands into our custom communication protocol, which utilizes the LoRa physical layer’s payload to transfer φ ’s x and y components (see Line 13). The current setup is limited to control and position commands.

To derive a map of the environment and to keep track of the robot within – in Line 13 – our approach uses a state-of-the-art SLAM algorithm from the literature [32]. The robot’s location is also used to determine whether the exploration is complete in Line 2. An earlier iteration of the work exploited a different SLAM algorithm from the visual SLAM community [37], showing that some of the components are interchangeable.

The software stack is distributed under the popular open-source CC BY-NC-SA license[†]. It is composed of three distinct components. (i) A “ground robot” ROS2 package implements the communication with a base station using either the IEEE 802.11 wireless communication or long-range LoRa technology. The package further contains serial communication with the microcontroller implemented in Arduino and the vertices detection (see Algorithm 1). (ii) A “ground navigation” ROS package collects point clouds from an RGB-D camera and other data from the SLAM algorithm [32] and ports them into ROS2. Finally, (iii) a “base server” implements the necessary functionality for remote human intervention. Both ground robot and ground navigation are implemented in C++ in ROS2 and ROS respectively, whereas base server is in PHP and JavaScript.

B. Low-cost hardware design

Our RB5 experimental robotic platform adopts a rocker-bogie suspension system [38] found on NASA’s rovers including Sojourner and Curiosity, which has compelling tradeoffs in terms of autonomy and obstacle avoidance (see Sec. IV). On either side of the robot, an upside-down V-shaped linkage called the rocker pivots about an axis on the robot frame. The rocker has a wheel at one end and a smaller V-shaped linkage on the other arm. The smaller linkage, called the bogie, can pivot about an axis on the rocker and has two wheels at its tips. The articulated nature of the rocker-bogie suspension allows the mobile robot to adapt to uneven terrains [6] as the rocker and bogie pivot to maintain wheel contact. Each of the six wheels in the rocker-bogie suspension is actuated by a DC gear motor, whereas the rotational degrees of freedom in the rocker-bogie suspensions are passive. Since the wheels are all parallel and cannot rotate out of the plane, the robot uses the same actuation strategy as that of a differential drive vehicle to move straight and make turns by controlling the left and right sets of wheels in the same and opposite directions. Given that RB5 has multiple wheels on each side, its ability to make turns is reduced compared to a differential drive vehicle. Due to its extended body length, RB5 incorporates a caster wheel in the back to support the rear end of the frame.

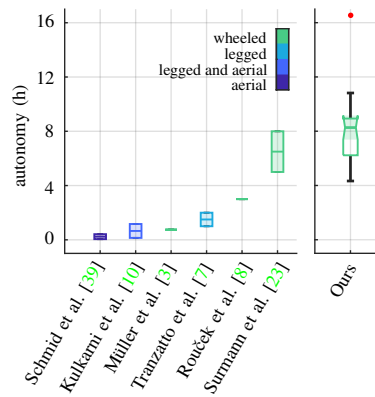


Fig. 3: **Autonomy for different classes of mobile robots.** Autonomy is reported in hours between the time the battery is fully charged to discharged for our RB5 explorer and other approaches that report the value in the literature. Even though the metric is use case- and battery-dependent, the data show that the reported autonomy for wheeled robots is higher than the reported autonomy for legged, combination of legged and aerial, and aerial robots.

The robot frame’s dimensions are 914 by 330 millimeters, and the robot’s bounding box dimensions are 991 by 762 mm. The frame consists of one-inch aluminum extrusions and acrylic sheets, and the rocker and bogie linkages are assembled from aluminum sheets and standoffs. The pivots of the bogie and rocker sit at 240 and 330 mm from the ground respectively, providing a clearance of approximately 190 mm beneath the frame, i.e., RB5 can clear obstacles passively up to 19 cm. The two wheels on each bogie linkage are coplanar, but the wheel on the corresponding rocker linkage is closer to the medial plane of the robot. Motor control is performed by a Teensy (R) 4.0 microcontroller board sending PWM commands to six DRV8871 motor driver boards. An onboard 24 volts LiFePO₄ battery provides power for the microcontroller, motor drives, and computing hardware.

IV. EXPERIMENTS

In order to demonstrate our approach, we conduct a set of field experiments involving our RB5 experimental robotic platform in a variety of environments, including indoor structured, unstructured underground, and outdoors. In each, the microcontroller executes a finite set of motion primitives via velocity control. These primitives are transmitted serially to the microcontroller from RB5’s onboard computing hardware, an NVIDIA (R) Jetson Xavier NX (TM) embedded board, which runs our autonomous exploration software stack. The computing hardware mounts peripherals for visual sensing and for communication. The former group consists of an Intel (R) RealSense (TM) D435 RGB-D camera, and the latter consists of a LoRa wireless network bundle with the RN2903 module and an Intel (R) AX200 network card for standard wireless communication via 802.11 protocol when, e.g., RB5 is in reach of an available wireless network. All the software components in charge of the exploration (detailed at the end of Sec. III-A) run in real-time onboard RB5. Additional processing is possible, e.g., via the ROS network.

Fig. 3 compares our hardware approach to others. “Autonomy,” which is related to instantaneous energy consumption, is reported in hours between the time the battery is fully charged to discharged – the time when the robot can actively explore its surroundings – and is compared to representative approaches in the literature tackling autonomous exploration. For our RB5, the minimum and maximum are approximately four hours and twenty minutes and sixteen and a half hours

when the robot respectively moves at full speed and is not moving (red outlier). The first quartile is six hours and ten minutes, the third is nine hours. The median is eight hours and twenty minutes when the average velocity is two-thirds of the maximum. Even though the metric is often use case- and battery-dependent (i.e., in [7, 8] the objective is to explore the surroundings in the shortest time), the data show that the reported autonomy for wheeled robots [8, 23] is generally higher than the reported autonomy for legged [7], combination of legged and aerial [10], and aerial robots [39]. Here [3] is an outlier as it uses a small wheeled robot.

Fig. 4 shows experimental results for a structured indoor environment, a university hallway on the second floor of a multistory building. The hallway is composed of four connected corridors for a total approximate length of 80 meters in a closed circuit. The resulting point cloud is shown in Fig. 4a, where the color scheme in the top-left indicates the different heights of points in the point cloud. Figs. 4b–4c show a detail of the algorithm in the experiment in terms of obstacle detection and avoidance. Here RB5 detects an obstacle, a “door” with a surrounding wall as it travels through the hallway at approximately 15 and 0 on the respective z- and x-axis. Fig. 4b shows the initial detection of the obstacle on top. The vertices V, O_i are the empty red circles and represent the field of view on the left and the edge of the obstacle on the right. On the bottom is the path-following vector field from Eq. (3) in red and the path function ϕ_t in cyan. Fig. 4c shows the following time step when the robot has to perform a sharper maneuver to avoid the obstacle.

Fig. 5 shows experimental results for an unstructured environment, a hallway connecting to an underground tunnel (in Fig. 1) on the respective left and right sides of Fig. 5a. The

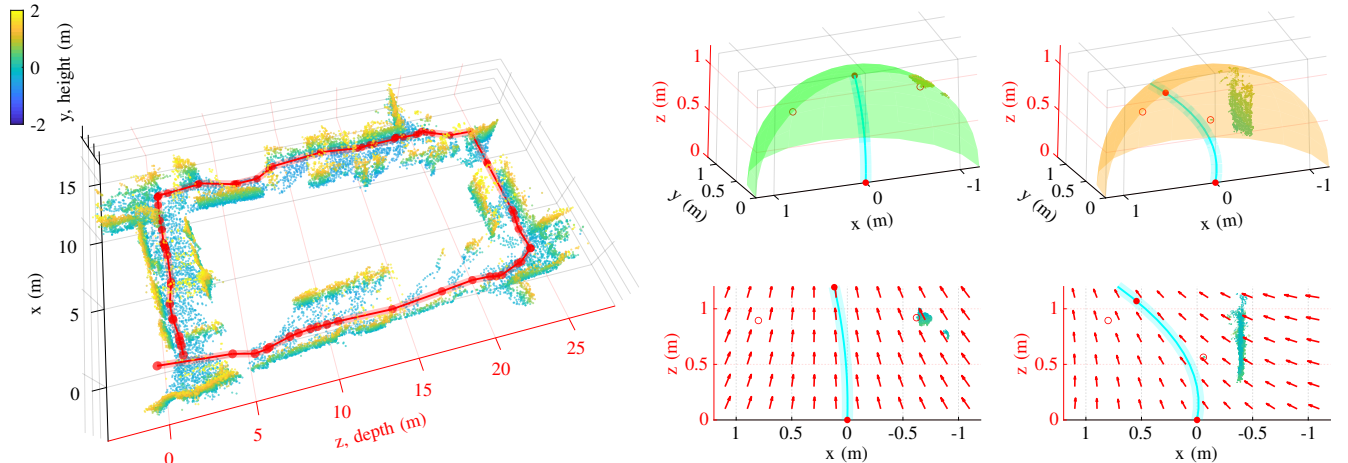
hallway and tunnel combined have an approximate length of 100 meters. Conversely to the experiment in Fig. 4, this experiment showcases an open circuit, i.e., the exploration is concluded when a specific frontier is encountered. Figs. 5b–5c show the obstacle detection, similar to Figs. 4b–4c, for a wheel placed close to the left edge of the first length of the figure wide approximately 0.42 meters. The trajectory of the robot avoiding the obstacle is to be observed in Fig. 5a between 15 and 20 meters on the z-axis. The figure also demonstrates the remote human intervention via LoRa, as the robot is stuck at the entrance of the underground tunnel (approximately 50 meters on the z-axis in Fig. 5a).

The turning direction E in Eq. (3) is positive for left turns (see Figs. 4b–4c) and negative for right turns (see Figs. 5c–5b). The turning rate k_e is derived empirically similar to other literature [29, 30] and is 0.05, 0.1, and 0.4 depending on the turning maneuver, i.e., it is 0.05 when ϕ_t is a line (or close to it), 0.4 when a sharp curve in respectively Fig. 4a and 5b, and 0.1 otherwise. The points in the point cloud are adjusted for height and length and filtered for visualization purposes, i.e., we have reported one point every 250, every 500, etc., in Fig. 4a and 5a.

V. LIMITATIONS OF A LOW-COST EXPLORER

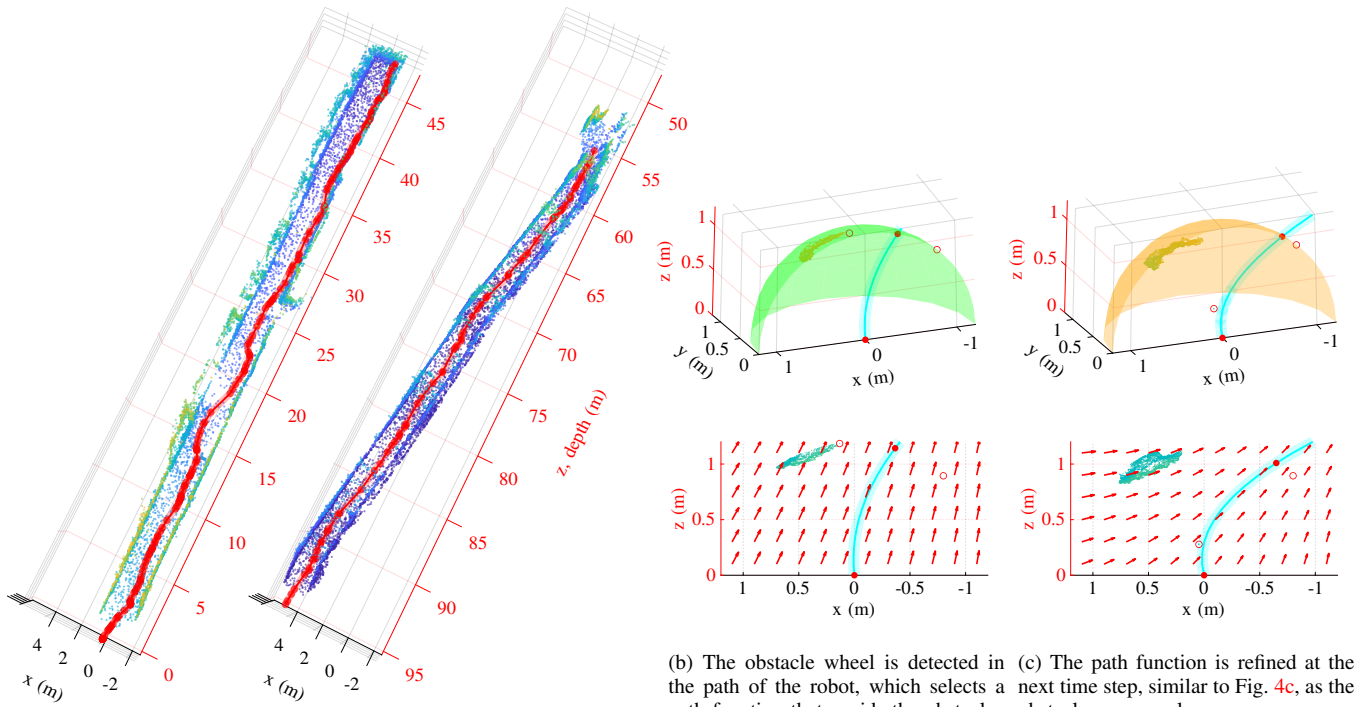
In this section, we discuss the limitations of the current approach from both software and hardware perspectives.

Software-wise, a negative of the low-cost approach is a reduced density of the point cloud, as visualized in Fig. 4, where between, e.g., 15 and 20 meters on the z-axis and zero and five meters on the x-axis there are significantly fewer points in the point cloud than in other parts of the figure. The algorithm here keeps track (see Line 13) of the path function ϕ_t (see Line 8) in the event of, e.g., the computing hardware



(a) Point cloud view of a structured indoor environment with visible contours of the exploration space. Points are colored for different heights. (b) The first detection of an obstacle. A path function is selected to avoid the obstacle. (c) The new path function is selected at the next time step as the obstacle occurrence is observed closer.

Fig. 4: **Results for a structured environment.** Experimental results are reported for a structured indoor environment, a university hallway composed of four connected corridors for a total length of approximately 80 meters. The view includes the point cloud in Fig. 4a and the detail of the algorithm for obstacle avoidance and detection at successive time steps in Fig. 4b and 4c. The points in the point cloud are filtered to report one point every 250. The colors of the spheres in Figs. 4b–4c indicate the proximity of an obstacle (orange indicates close proximity) and arrows the path-following vector field in Eq. (3). The robot’s trajectory is in red and red dots indicate SLAM’s registration points.



(a) Point cloud view of an unstructured indoor environment (left) and an underground tunnel (right) with visible contours of the exploration space. The color scale is the same as in Fig. 4a.

Fig. 5: **Results for an unstructured environment.** Experimental results are reported for an unstructured indoor environment and an underground tunnel for a total length of approximately 100 meters. The view of the point cloud in Fig. 5a is filtered to report one point every 500. The detail of the algorithm for successive time steps is shown in Figs. 5b–5c, similar to Fig. 4.

being busy while executing other tasks such as communication. While specific to the computing hardware onboard RB5, the occurrence is expected with lower-performing computing hardware. It is due to the unpredictable nature of the execution, which is a common occurrence in the literature, especially if involving heterogeneous elements, i.e., CPU, GPU, and microcontrollers [40]. Despite a lower update frequency, the approach maintains its obstacle avoidance and navigation capabilities, with a nominal frequency of one to ten hertz.

Hardware-wise, a hurdle that we encountered is that many components are still expensive and limited in variety. Prior work has been opting for expensive servo motors or well-established electric motor manufacturers. Furthermore, existing low-cost kits such as the TurtleBot [35] are limited to deployment in environments that are not physically demanding. There is still a large gap in low-cost robot hardware that can be tested in challenging conditions. Due to the lack of a common specification for a rough terrain environment, there are no performance or life cycle requirements to meet in the design process; therefore, it is difficult to develop a low-cost generalized mobile robot for rough terrains.

VI. CONCLUSION AND FUTURE DIRECTIONS

This paper consists of an approach and an experimental robotic platform for low-cost autonomous long-term exploration in both indoor and outdoor environments. While comparable with other approaches tackling autonomous ex-

ploration, our approach operates in the presence of fewer sensory and computing requirements. Requiring only an RGB-D camera, all the exploration is computed in real-time on low-power computing hardware that is cheaper compared to the existing literature in similar settings.

The exploration consists of a mixed approach – a frontier and sampling-based method from the literature extended with a path-following vector field from the aerial robotics domain – which allows the robot to operate at lower update frequencies. The position is from a state-of-the-art SLAM algorithm. Human intervention, if required, is implemented via a novel methodology based on the LoRa low-power long-range communication technology from the internet-of-things domain. Requiring only two low-cost LoRa bundles for communication, the approach enables operations on long distances with a custom communication protocol with no significant impact on price and resources as opposed to existing methodologies based on a mesh of devices.

To enable further savings, we are currently extending the approach to account for energy requirements and to different cost functions in Eq. (7). Applicability to different use cases is also being investigated via, e.g., implementation of feature detection and tracking and extension of the custom LoRa communication protocol.

ACKNOWLEDGMENTS

We thank Paedyn Gomes, Victoria Ereskina, and Beau Birdsall for their contribution to the mechanical design.

REFERENCES

- [1] I. Lluvia, E. Lazkano, and A. Ansuategi, "Active mapping and robot exploration: A survey," *Sensors*, vol. 21, no. 7, p. 26, 2021. **1**
- [2] J. A. Placed, J. Strader, H. Carrillo *et al.*, "A survey on active simultaneous localization and mapping: State of the art and new frontiers," *IEEE Transactions on Robotics*, vol. 39, no. 3, pp. 1686–1705, 2023. **1, 2**
- [3] M. Müller and V. Koltun, "OpenBot: Turning smartphones into robots," in *International Conference on Robotics and Automation (ICRA)*. IEEE, 2021, pp. 9305–9311. **1, 2, 4, 5**
- [4] B. Zhou, Z. Wu, and X. Liu, "Smartphone-based robot indoor localization using inertial sensors, encoder and map matching," in *International Conference on Automation, Control and Robots (ICACR)*. IEEE, 2021, pp. 145–149. **1**
- [5] S. Srinivasa, P. Lancaster, J. Michalove *et al.*, "MuSHR: A low-cost, open-source robotic racecar for education and research," p. 4, 2019, arXiv preprint, doi.org/10.48550/arXiv.1908.08031. **1**
- [6] S. M. F. Faisal, T. Rahman, and M. A. Kabir, "A low-cost rough terrain explorer robot fabrication using rocker bogie mechanism," in *International Conference on Computer, Communication, Chemical, Materials and Electronic Engineering (IC4ME2)*. IEEE, 2021, p. 4. **1, 2, 4**
- [7] M. Tranzatto, F. Mascariich, L. Bernreiter *et al.*, "CERBERUS: Autonomous legged and aerial robotic exploration in the tunnel and urban circuits of the DARPA Subterranean Challenge," *Field Robotics*, vol. 2, pp. 274–324, 2022. **1, 4, 5**
- [8] T. Rouček, M. Pecka, P. Čížek *et al.*, "DARPA Subterranean Challenge: Multi-robotic exploration of underground environments," in *International Conference on Modelling and Simulation for Autonomous Systems (MESAS)*. Springer, 2020, pp. 274–290. **1, 4, 5**
- [9] W. Tabib, K. Goel, J. Yao *et al.*, "Autonomous cave surveying with an aerial robot," *IEEE Transactions on Robotics*, vol. 38, no. 2, pp. 1016–1032, 2022. **1**
- [10] M. Kulkarni, M. Dharmadhikari, M. Tranzatto *et al.*, "Autonomous teamed exploration of subterranean environments using legged and aerial robots," in *International Conference on Robotics and Automation (ICRA)*. IEEE, 2022, pp. 3306–3313. **1, 4, 5**
- [11] K. Ebadí, Y. Chang, M. Palieri *et al.*, "LAMP: Large-scale autonomous mapping and positioning for exploration of perceptually-degraded subterranean environments," in *International Conference on Robotics and Automation (ICRA)*. IEEE, 2020, pp. 80–86. **1**
- [12] K. Ismail, R. Liu, J. Zheng *et al.*, "Mobile robot localization based on low-cost LTE and odometry in GPS-denied outdoor environment," in *International Conference on Robotics and Biomimetics (ROBIO)*. IEEE, 2019, pp. 2338–2343. **1**
- [13] F. Voigtländer, A. Ramadan, J. Eichinger *et al.*, "5G for robotics: Ultra-low latency control of distributed robotic systems," in *International Symposium on Computer Science and Intelligent Controls (ISCSIC)*. IEEE, 2017, pp. 69–72. **1**
- [14] C. Delgado, L. Zanzi, X. Li *et al.*, "OROS: Orchestrating ROS-driven collaborative connected robots in mission-critical operations," in *International Symposium on a World of Wireless, Mobile and Multimedia Networks (WoWMoM)*. IEEE, 2022, pp. 147–156. **1**
- [15] C. Cadena, L. Carlone, H. Carrillo *et al.*, "Past, present, and future of simultaneous localization and mapping: Toward the robust-perception age," *IEEE Transactions on Robotics*, vol. 32, no. 6, pp. 1309–1332, 2016. **1**
- [16] A. Eldemiry, Y. Zou, Y. Li *et al.*, "Autonomous exploration of unknown indoor environments for high-quality mapping using feature-based RGB-D SLAM," *Sensors*, vol. 22, no. 14, p. 16, 2022. **1**
- [17] M. Corah, C. O'Meadhra, K. Goel *et al.*, "Communication-efficient planning and mapping for multi-robot exploration in large environments," *IEEE Robotics and Automation Letters*, vol. 4, no. 2, pp. 1715–1721, 2019. **1**
- [18] J. P. Shanmuga Sundaram, W. Du, and Z. Zhao, "A survey on LoRa networking: Research problems, current solutions, and open issues," *IEEE Communications Surveys & Tutorials*, vol. 22, no. 1, pp. 371–388, 2020. **1, 4**
- [19] D. Tardioli, L. Riazuelo, D. Sicignano *et al.*, "Ground robotics in tunnels: Keys and lessons learned after 10 years of research and experiments," *Journal of Field Robotics*, vol. 36, no. 6, pp. 1074–1101, 2019. **1**
- [20] T. Dang, F. Mascariich, S. Khattak *et al.*, "Graph-based path planning for autonomous robotic exploration in subterranean environments," in *International Conference on Intelligent Robots and Systems (IROS)*. IEEE, 2019, pp. 3105–3112. **1, 2**
- [21] A. Batinovic, T. Petrovic, A. Ivanovic *et al.*, "A multi-resolution frontier-based planner for autonomous 3D exploration," *IEEE Robotics and Automation Letters*, vol. 6, no. 3, pp. 4528–4535, 2021. **1, 2**
- [22] H. Kim, H. Kim, S. Lee *et al.*, "Autonomous exploration in a cluttered environment for a mobile robot with 2D-map segmentation and object detection," *IEEE Robotics and Automation Letters*, vol. 7, no. 3, pp. 6343–6350, 2022. **1**
- [23] H. Surmann, A. Nüchter, and J. Hertzberg, "An autonomous mobile robot with a 3D laser range finder for 3D exploration and digitalization of indoor environments," *Robotics and Autonomous Systems*, vol. 45, no. 3, pp. 181–198, 2003. **1, 2, 4, 5**
- [24] A. Bircher, M. Kamel, K. Alexis *et al.*, "Receding horizon "next-best-view" planner for 3D exploration," in *International Conference on Robotics and Automation (ICRA)*. IEEE, 2016, pp. 1462–1468. **1, 2**
- [25] A. Dai, S. Papatheodorou, N. Funk *et al.*, "Fast frontier-based information-driven autonomous exploration with an MAV," in *International Conference on Robotics and Automation (ICRA)*. IEEE, 2020, pp. 9570–9576. **1, 2**
- [26] J. Betz, H. Zheng, A. Liniger *et al.*, "Autonomous vehicles on the edge: A survey on autonomous vehicle racing," *IEEE Open Journal of Intelligent Transportation Systems*, vol. 3, pp. 458–488, 2022. **1, 2**
- [27] R. Shrestha, F.-P. Tian, W. Feng *et al.*, "Learned map prediction for enhanced mobile robot exploration," in *International Conference on Robotics and Automation (ICRA)*. IEEE, 2019, pp. 1197–1204. **1, 2**
- [28] W. Qiao, Z. Fang, and B. Si, "A sampling-based multi-tree fusion algorithm for frontier detection," *International Journal of Advanced Robotic Systems*, vol. 16, no. 4, p. 14, 2019. **2**
- [29] A. Seewald, H. García de Marina, H. S. Midtiby *et al.*, "Energy-aware planning-scheduling for autonomous aerial robots," in *International Conference on Intelligent Robots and Systems (IROS)*. IEEE, 2022, pp. 2946–2953. **2, 5**
- [30] H. García de Marina, Y. A. Kapitanyuk, M. Bronz *et al.*, "Guidance algorithm for smooth trajectory tracking of a fixed wing UAV flying in wind flows," in *International Conference on Robotics and Automation (ICRA)*. IEEE, 2017, pp. 5740–5745. **2, 3, 5**
- [31] A. Seewald, "Energy-aware coverage planning and scheduling for autonomous aerial robots," Ph.D. thesis, Syddansk Universitet, 2021, doi.org/10.21996/7ka6-r457.2
- [32] M. Labbé and F. Michaud, "RTAB-Map as an open-source LiDAR and visual simultaneous localization and mapping library for large-scale and long-term online operation," *Journal of Field Robotics*, vol. 36, no. 2, pp. 416–446, 2019. **2, 4**
- [33] T. P. Setterfield and A. Ellery, "Terrain response estimation using an instrumented rocker-bogie mobility system," *IEEE Transactions on Robotics*, vol. 29, no. 1, pp. 172–188, 2013. **2**
- [34] S. Kirchgeorg and S. Mintchev, "Multimodal aerial-tethered robot for tree canopy exploration," in *International Conference on Intelligent Robots and Systems (IROS)*. IEEE, 2022, pp. 6080–6086. **2**
- [35] R. Amsters and P. Slaets, "TurtleBot 3 as a robotics education platform," in *International Conference on Robotics in Education (RiE)*. Springer, 2020, pp. 170–181. **2, 6**
- [36] V. M. Goncalves, L. C. A. Pimenta, C. A. Maia *et al.*, "Vector fields for robot navigation along time-varying curves in n -dimensions," *IEEE Transactions on Robotics*, vol. 26, no. 4, pp. 647–659, 2010. **2**
- [37] C. Campos, R. Elvira, J. J. G. Rodríguez *et al.*, "ORB-SLAM3: An accurate open-source library for visual, visual-inertial, and multimap SLAM," *IEEE Transactions on Robotics*, vol. 37, no. 6, pp. 1874–1890, 2021. **4**
- [38] D. B. Bickler, "Articulated suspension system," U.S. Patent 4 840 394, June 20, 1989. **4**
- [39] L. Schmid, M. Pantic, R. Khanna *et al.*, "An efficient sampling-based method for online informative path planning in unknown environments," *IEEE Robotics and Automation Letters*, vol. 5, no. 2, pp. 1500–1507, 2020. **4, 5**
- [40] A. Seewald, U. P. Schultz, E. Ebeid *et al.*, "Coarse-grained computation-oriented energy modeling for heterogeneous parallel embedded systems," *International Journal of Parallel Programming*, vol. 49, no. 2, pp. 136–157, 2021. **6**